https://doi.org/10.1016/j.electacta.2016.06.059

Flexible fiber hybrid supercapacitor with $NiCo_2O_4$ nanograss@carbon fiber and bio-waste derived high surface area porous carbon

S. T. Senthilkumar[a], Nianqing Fu[a], Yan Liu[a], Yu Wang[b], Limin Zhou[c] and Haitao Huang[a]*

[a] Department of Applied Physics, The Hong Kong Polytechnic University, Hong Kong SAR, China.
[b] School of Materials Science and Engineering, Nanchang University, Jiangxi 330031, China
[c] Department of Mechanical Engineering, The Hong Kong Polytechnic University, Hong Kong SAR, China.

*Corresponding author. Tel.: +852 27665694; fax: +852 2333 7629.
Email address: aphhuang@polyu.edu.hk (H. Huang).

Abstract

Flexible, light weight and portable energy storage devices are receiving much attention for flexible electronic applications. Nonetheless, these conventional two-dimensional (2D) or planar structured flexible energy storage devices could not meet the demand for wearable or textile electronics. To meet this demand, in this work, a novel flexible fiber hybrid supercapacitor (HSC) is fabricated using $NiCo_2O_4$ nanograss (NG)-array coated carbon fiber ($NiCo_2O_4$ NG@CF) as the positive electrode to provide a pseudocapacitance and porous carbon coated carbon fiber electrode as the negative electrode to provide an electric double-layer capacitance (EDLC). Particularly, the porous carbon is prepared from *Lemon peel waste* to obtain a low cost electrode material. Interestingly, the fabricated HSC exhibits a maximum specific capacitance of 17.5 F g^{-1} (25.03 mF cm^{-2})) and an energy density of 6.61 Wh kg^{-1} (9.46 μWh cm^{-2}) at the current of 1 mA, which is far better than previous reports. Moreover, three knitted fiber HSCs connected in series could successfully power up a red LED, even at a folded condition. It is believed that this type of fiber HSC could be a potential candidate for flexible/wearable electronic applications.

Keywords: Flexible, Wearable, Fiber Supercapacitor, Capacitance, Energy density

1. Introduction

Flexibility is among the most important requirements in today's advanced wearable electronic applications. Recently, flexible supercapacitors (SCs) have attracted much attention as electrochemical energy storage devices because of their high power density, good cyclic performance and safety as compared with batteries, and high energy density as compared with classical dielectric capacitors [1,2]. To enable the integration of flexible SCs into textiles/wearable electronics, fiber based SCs are designed and have received intensive study since they can provide more flexibility than planar type SCs and can be easily woven into fabrics with desired shape. Many of the recently developed symmetric fiber SCs are based on carbon materials, such as carbon nanotubes (CNTs) [3], graphene [4], carbon nanofibers [5,6] carbon ink [7] and graphene/CNT [8]. To improve the specific capacitance and energy density, some metal oxides ($NiCo_2O_4$ and $ZnCo_2O_4$) [9,10] and composite materials (MnO_2/ZnO nanowires (NGs) [11], Bi_2O_3/graphene [12], MnO_2/graphene [13], CNT/Polyaniline (PANI) [14] and so on) are explored. Regrettably, the achieved energy density of previously reported fiber SCs are still low. Particularly, the low voltage is a major cause for the low specific energy of these carbon based SCs.

To this end, fiber hybrid supercapacitors (HSCs) using two types of electrodes with different working potentials were developed and a high energy density (E=0.5CV^2, where C is the capacitance and V is the working voltage) can be achieved due to the high cell voltage based on the asymmetric configuration [15]. But the metal or conductive material coated plastic wires which were used as fiber electrodes in the earlier reports [2,16–19] were not flexible enough for wearable devices, making the devices easily broken during bending, and those fiber electrodes were also heavy, offering additional weight to the devices. Recently, carbon fibers (CFs) have been considered as attractive alternative current collectors (coated with active materials [2]) due to their excellent flexibility, high strength, good electrical

conductivity, inert nature under ambient conditions and low price [4] that make them applicable in the design of novel fiber HSCs. In addition, using pseudocapacitive material with high capacitance is an effective way to further improve the energy performance of fiber HSCs. Among the pseudocapacitive electrode materials, mixed transition-metal oxides ($NiCo_2O_4$, $ZnCo_2O_4$, and $NiMoO_4$, etc.,) are promising due to their good electrochemical properties, such as good reversibility and conductivity [20,21].

Moreover, porous carbon is considered as excellent electrode material for SCs owing to its large surface area, controllable pore structure, good thermal and chemical stability, and low cost [22]. Several methods have been used to prepare the porous carbon. Among them, hydrothermal carbonization (HTC) is attractive since it can control the pore structure of carbon to achieve good capacitive performance [23]. Bio-waste is an eco-friendly precursor for the porous carbon, which is rich in carbon content because it consists of biopolymers (i.e., cellulose, hemicelluloses and lignin) [24]. In the present work, lemon peel was used to prepare the porous carbon using the HTC method, associated with activation of carbon. This is an economical way to produce porous carbon since, generally, lemon is cultivated for its juice, while the outer lemon peel is considered as waste and is available over the year. The lemon waste derived porous carbon was used as low cost and high performance negative electrode for HSCs.

Herein, we designed and fabricated a novel flexible fiber HSC using $NiCo_2O_4$ nanograss (NG)@Carbon fiber ($NiCo_2O_4$ NG@CF) positive electrode and porous carbon coated CF negative electrode with polyvinyl alcohol (PVA)/KOH gel electrolyte. The fabricated HSC showed a maximum specific capacitance of 17.5 F g^{-1} (5.65 mF cm^{-1}) at a current of 1 mA and an energy density of 6.61 Wh kg^{-1} (9.46 μWh cm^{-2}) at a power density of 425.26 W kg^{-1} (608.4 μW cm^{-2}). Furthermore, about ~92% of the initial capacitance of HSC was retained after 3000 charge-discharge cycles.

2. Experimental

2.1. Synthesis of $NiCo_2O_4$ NG@CF

$NiCo_2O_4$ was grown on CFs using a hydrothermal method where the CFs act as supporting backbone for controlled growth of $NiCo_2O_4$ NGs. In a typical synthesis, 1.2 mmol of $Ni(NO_3)_2{\cdot}6H_2O$ and 2.4 mmol of $Co(NO_3)_2{\cdot}6H_2O$ were initially added into 40 mL of distilled water under stirring. Then 2.2 mmol of NH_4F and 5.3 mmol of urea were added into the above solution during stirring and this mixed solution was kept for a few minutes. Afterwards, the resulted solution was transferred into a Teflon-lined stainless steel autoclave with pre-cleaned carbon fibers (CFs) and kept at 130 °C for 5 h, followed by cooling to room temperature. After the hydrothermal treatment, the CFs were taken out, washed with distilled water and ethanol for several times and dried in air at 60 °C for overnight. Finally, the dried samples were calcined at 300 °C for 4 h under N_2 atmosphere to obtain the $NiCo_2O_4$ NG@CF (the reaction mechanism being given in Supporting Information) which was used as the positive fiber electrode in a fiber HSC.

2.2. Synthesis of porous carbon

The highly porous carbon was derived from *lemon peel* by simple hydrothermal carbonization combined with activation. In details, lemon waste and 80 mL distilled water were placed into a Teflon-lined stainless steel autoclave, sealed, and heated at 180 °C for 24 h, followed by cooling to room temperature. Then, the resulted sample was washed with distilled water and dried. For the carbonization process, 5 g of hydrothermally treated sample was chemically activated using 20% KOH and carbonized in a tube furnace at 800 °C for 3 h under N_2 atmosphere. Subsequently, the activated sample was thoroughly washed with desired amount of HCl and distilled water, followed by drying at 60 °C overnight to obtain the porous activated carbon power.

2.3. Fabrication of fiber HSC

To prepare the polyvinyl alcohol (PVA)/KOH gel electrolyte, 1 g of PVA was dissolved in 20 mL of distilled water at 70 °C under stirring and then 2 M of KOH solution was added dropwise while stirring. After that, the mixed solution was kept for 2 h until a clear gel-like solution was obtained. Both the $NiCo_2O_4$@CF and porous carbon coated CF electrodes were immersed into the PVA/KOH gel electrolyte for one minute and dried at 60 °C for 5 minutes. Subsequently, the fiber electrodes were again immersed into the PVA/KOH gel electrolyte, twisted together and dried at room temperature to obtain the fiber HSC. The length of the fabricated fiber supercapacitor was 6 cm.

2.4. Material characterization

The XRD patterns of the $NiCo_2O_4$@CFs and porous carbon were obtained with Bruker D8 Discover X-diffractometer using Cu-K_α radiation. Scanning electron microscopy (SEM) and transmission electron microscopy (TEM) were recorded on FESEM (FEI Nov Nano SEM) and JEOL (JEM-2100F), respectively. Raman spectrum was recorded using a Jobin-Yavon T6400 micro-Raman system with an Ar laser. Specific surface area was calculated from the N_2 physisorption results measured at 77 K (Micromeritics ASAP 2020) by using the BET (Brunauer–Emmet–Teller) method. The electrochemical properties of individual electrode ($NiCo_2O_4$@CF and porous carbon coated fiber electrodes) were measured in 2M KOH using a three-electrode system, where Hg/HgO and Pt-plate were used as reference and counter electrodes, respectively. Similarly, the electrochemical performances of the fabricated fiber HSCs were studied in a two-electrode system with the $NiCo_2O_4$@CF as the positive electrode and the porous carbon coated CF as the negative electrode. The cyclic voltammetry, galvanostatic charge-discharge and cyclic life measurements were performed using CHI 660 E electrochemical workstation.

3. Results and discussion

3.1. Characterization

Fig. 1 presents a schematic illustration of the proposed fiber HSC where the $NiCo_2O_4$@CF fiber electrode was used as the positive electrode and the lemon-peel-derived porous carbon coated CF was used as the negative electrode. The fiber HSC was fabricated by twisting the two electrodes together with PVA/KOH gel acting as both the electrolyte and the separator to avoid the short-circuit between the positive and negative electrodes.

Fig. 2a shows that the as-prepared $NiCo_2O_4$ NGs are uniformly and densely grown on CFs, with a diameter ~55-80 nm (Fig. 2b). The one-dimensional NGs are expected to contribute significantly to the high capacitance and the high power because of their large active surface area for electrolytic ions and one dimensional charge transport [11]. The inset in Fig. 2a shows a photo of the prepared $NiCo_2O_4$@CF sample, exhibiting excellent flexibility, ready to be woven into fabrics. Moreover, neighboring $NiCo_2O_4$ NGs are joined together at the tips of NGs to form bundles of NGs (Fig. 2c and 2d). The as-prepared carbon shows a highly porous structure (Fig. 2e and 2f) with highly accessible and interconnected pores for the easy infiltration of electrolyte and good electrolyte wettability is expected [22].

Fig. 3a is a low-magnification TEM image of a typical $NiCo_2O_4$ NG, showing a porous structure with many small nanoparticles, which is ascribed to the thermal decomposition of the $NiCo_2O_4$ precursor (see Supporting Information for details). The prepared $NiCo_2O_4$ NG has a sharp edge (inset of Fig. 3a) and a broad base (Fig. 3a). Fig. 3b shows the high resolution TEM (HR-TEM) image of spinel $NiCo_2O_4$, revealing the (220), (311) and (400) planes with the corresponding interplanar *d*-spacing of 0.28, 0.25 and 0.19 nm, respectively. All the diffraction rings shown in the selected area electron diffraction (SAED) pattern (inset of Fig. 3b) can be well indexed to the spinel $NiCo_2O_4$ structure, agreeing well with the standard lattice parameters (JCPDS No: 20-0781). Fig. 3c and 3d

depict the porous structure of the prepared carbon sample, showing micropores and disordered graphitic carbon [25].

Fig. 4a shows the XRD pattern of the as-prepared $NiCo_2O_4$@CFs and porous carbon. All the diffraction peaks ((111), (220), (311), (400), (511) and (440)) in Fig. 4a can be indexed to the spinel $NiCo_2O_4$ crystalline structure (JCPDS No: 20-0781) and no other peaks were found, except a broad peak arising from the CF substrate at 21-30°. The relatively broad peaks of $NiCo_2O_4$ reveal the small crystallite size or low crystallinity [26,27]. The two broad peaks of the as-prepared carbon (Fig. 4a) are indexed as (002) and (100) of the pseudo-graphitic carbon, indicative of disordered carbon structure [25]. This result was supported by the Raman spectra (Fig. S1, Supporting Information). Two prominent Raman peaks are observed at 1363 and 1598 cm^{-1}, corresponding to a disordered D-band carbon and an sp^2 hybridized G-band carbon of an aromatic structure or a graphitic nature, respectively [25]. The surface area of the as-prepared porous carbon is 1012 m^2/g, as measured by the N_2 adsorption-desorption isotherm (Fig. S2, Supporting Information).

The species and chemical states of different elements of $NiCO_2O_4$ NG@CFs were also analyzed via X-ray photoelectron spectroscopy (XPS) as shown in Fig. 4b-d. The survey spectrum (Fig. S3a, Supporting Information) shows the existence of Ni, Co C, and O elements (where the C came from CFs), without any impurities. The de-convoluted Co 2p displays the electronic configuration of Co atoms in $2P_{1/2}$ and $2P_{2/3}$ states at 794.86 and 779.44 eV, respectively (Fig. 4b). The fitting peaks at 778.98 and 794.2 eV are indexed to Co^{3+}, while the other two fitting peaks at 780.8 and 796.2 eV belong to Co^{2+} [28]. The de-convoluted Ni 2p peaks shows the electronic configuration of Ni atoms in $2P_{1/2}$ and $2P_{2/3}$ states at 872.26 and 855.07 eV, respectively (Fig. 4c). The fitting peaks at 853.9 and 871.7 eV are attributed to Ni^{2+}, while the other fitting peaks at 855.78 and 873.3 eV are ascribed to Ni^{3+} [28]. Moreover, satellite speaks (indicated as Sat.) are observed in both Co 2p (Fig. 4b)

and Ni 2p (Fig. 4c) spectra. The three fitting peaks of O 1s (Fig. 4d) correspond to metal oxygen (M-O-M) (peak 1), C=O (peak 2) [26] and O–C=O bonds (peak 3) at 529.19, 532.65, and 530.86 eV, respectively, which come from the oxygen groups of CFs. The XPS survey spectrum of the porous carbon is shown in Fig. S3b (Supporting Information). The C 1s peak (Fig. 4e) of the porous carbon was de-convoluted into three peaks, corresponding to the signal of C=C–C (284.57 eV (C_1)), C–O (286 eV (C_2)), and O–C=O bonds (289.5 eV (C_3)) [25,29]. Similarly, the O 1s peak (Fig. 4f) was also de-convoluted into three peaks at 531.5 (O_1), 533.18 (O_2) and 536.03 eV (O_3), which correspond to the signal of C=O and C–OH bonds, and chemisorbed water [25,29].

3.2. Electrode Performance

Cyclic voltammetry (CV) and galvanostatic charge-discharge (GCD) were employed in a three-electrode system to investigate the electrochemical properties of the $NiCo_2O_4$@CF electrode and the porous carbon coated CF electrode. Fig. 5a shows the CV curves of $NiCo_2O_4$@CF electrode tested in 2M KOH at different scan rates (0.2–2 mV s^{-1}), in a potential range from 0 to 0.65 V *vs* Hg/HgO. A typical oxidation peak during the anodic process and a reduction peak during the cathodic process are observed, indicative of the pseudocapacitive nature of the electrode due to the Faradaic redox reactions of Ni and Co species in KOH electrolyte. The observed peak potentials are centered at ~0.51 V (P_1) and ~0.33 V (P_2) *vs* Hg/HgO, respectively, at a scan rate of 0.3 mV s^{-1}. The corresponding redox reactions of $NiCo_2O_4$ with OH anions are governed by the following equations [30,31],

$$NiCo_2O_4 + OH^- + H_2O \leftrightarrow NiOOH + 2CoOOH + 2e^- \quad (1)$$

$$CoOOH + OH^- \leftrightarrow 4CoO_2 + H_2O + e^- \quad (2)$$

When the scan rate is increased, the anodic peak shifts toward more positive potentials and the cathodic peak shifts toward more negative potentials, due to the limited diffusion of OH^- at high scan rates. This quasi-reversible characteristics (or polarization effect of the electrode)

of the redox couples are common to pseudocapacitive electrode materials [32,33]. As seen from Fig. 5b, the CV curves of porous carbon coated fiber electrode (in a potential range from 0 to −1 V *vs* Hg/HgO at different scan rates (0.3–2 mV s^{-1})) are nearly rectangular, characteristic of an electrical double-layer capacitance (EDLC) due to the adsorption-desorption of electrolytic ions on the surface of electrode material [19]. Moreover, the CV curve remains rectangular with increasing scan rates, indicating the quick charge/discharge ability of the electrode [16].

Similarly, the charge-discharge behaviors of the $NiCo_2O_4$ NG@CF and the porous carbon coated fiber electrodes were tested in the potential ranges from 0 to 0.65 V and from 0 to −1 V *vs* Hg/HgO, respectively. Fig. 5c shows that, for the $NiCo_2O_4$ NG@CF fiber electrode, there is a noticeable voltage plateau (nonlinear discharge curve) in the discharge curve, a pseudocapacitive behavior of $NiCo_2O_4$. However, for the porous carbon coated fiber electrode, the discharge curve is linear (Fig. 5d) with time, indicating the EDLC of porous carbon. Herein, the specific capacitances of the electrodes are calculated using [25], $C = \frac{I\Delta t}{m\Delta V}$, where I is the applied current (mA), Δt is the discharge time (s), m is the mass of active electrode material (mg) and ΔV is the potential window (V). Fig. 5e displays the relation between specific capacitance and applied current. The calculated specific capacitances of the $NiCo_2O_4$ NG@CF fiber electrode are 735.9, 657, 596, 512.8 and 403 F g^{-1} at 1, 1.25, 1.5, 2 and 2.5 mA (0.16, 0.20, 0.25, 0.33 and 0.41 mA cm^{-1}), respectively. The obtained maximum capacitance of the $NiCo_2O_4$ NG@CF fiber electrode, 735.9 F g^{-1}, is appreciably higher than most of the previously reported values [34–38]. The charge storage processes of the $NiCo_2O_4$ NG@CF structure for effective electrochemical utilization are schematically illustrated in Fig. 5f. The excellent electrochemical properties of the $NiCo_2O_4$ NG@CF electrode can be attributed to the following aspects: (a) The 1D NG arrays could

provide short pathways for the ion diffusion and rapid charge collection/transfer. Besides, the $NiCo_2O_4$ NGs grown radially outward the CFs have good electrical connection with CFs which provide a reliable conductive network for fast electron transport throughout the electrode. Consequently, a large pseudocapacitance can be achieved. (b) The porous nanostructure of $NiCo_2O_4$ NGs also provides more electro-active sites for easy access of the electrolyte ions. These factors endow the $NiCo_2O_4$ NG@CF electrode with excellent electrochemical properties, such as high capacitance and good rate capability. The specific capacitances of the porous carbon fiber electrode are 213, 203.7, 193.5, 184 and 172.5 F g^{-1} at 1, 1.25, 1.5, 2 and 2.5 mA (0.16, 0.20, 0.25, 0.33 and 0.41 mA cm^{-1}), respectively. The specific capacitances of both electrodes decrease with increasing current, (Fig. 5d) due to the limited diffusion of electrolytic ions on the surface of or inside the electrodes.

3.3. Fiber Hybrid Supercapacitor (HSC) Performances

Fig. 6a shows that the $NiCo_2O_4$ NG@CF fiber electrode has a stable potential window from 0 to 0.65 V and the porous carbon fiber electrode has a stable potential window from 0 to −1 V. Hence it is possible to obtain a cell voltage of 1.65 V if the two electrodes are assembled to form a fiber HSC, as the total working voltage of a cell is the sum of the potential window of each electrode. To ensure equal amounts of charges (capacitances) on both electrodes, the optimal mass ratio of $NiCo_2O_4$ and porous carbon is calculated to be about 0.44 (details can be found in Supporting Information), based on the equation $\frac{m-}{m^+} = \frac{C^+ \times \Delta V^+}{C^- \times \Delta V^-}$ [19], where, m, C and ΔV are the mass of active material, gravimetric capacitance and potential window of the electrode, respectively (+ and – refer to positive and negative electrodes, respectively). Fig. 6b, displays the photo image of fabricated fiber HSC at normal and bending states, showing good flexibility of the device. Fig. 6c displays the schematic image of the fabricated fiber HSC, showing the electrode material's morphology and the corresponding electrochemical reactions on the positive and negative electrodes during charge-discharge. Fig. 6d and 6e

show that the fabricated fiber HSC can operate within the voltage range of 1.65 V. When the voltage is increased from 0.8 to 1.65 V, there is no predominated evolution region in the CV curves and no overcharging region in the GCD curves, revealing good electrochemical operation stability of the device [19]. Moreover, the device capacitance increases linearly with voltage, i.e., from 9 (2.91) to 17.5 F g^{-1} (5.65 mF cm^{-1}) when the voltage is increased from 0.8 to 1.65 V (Fig. S3, Supporting Information).

Fig. 7a shows that the fiber HSC has CV curves of the rectangle-like shape when the scan rate increases from 10 to 50 mV/s, revealing the rapid *I-V* response. Fig. 7b displays the typical triangular shape of the GCD curves of the HSC, indicating good electrochemical reversibility and good Columbic efficiency. The obtained maximum capacitances are 17.5 F·g^{-1} (5.65 mF cm^{-1}; 25.03 mF cm^{-2}) at 1 mA and 11.24 F g^{-1} (3.63 mF cm^{-1}; 5.3 mF cm^{-2}) at 3 mA (Fig. 7c). The fiber HSC exhibits both high energy density and high power density, which are 6.61 Wh kg^{-1} and 425 W kg^{-1} (Fig. 7d), respectively. As the current increases from 1 to 3 mA, the specific energy decreases from 6.61 to 4.25 Wh kg^{-1}, while the specific power increases from 425 to 1276 W kg^{-1}, where the achieved energy density is much higher than that of the symmetric porous carbon||porous carbon supercapacitor (0.83 Wh kg^{-1}, Fig. S4, Supporting Information). The obtained energy density is also higher than (or comparable with) those of the many reported planar-type HSCs, such as, MnO_2||PANI (5.86 Wh kg^{-1}) [39], MnO_2||PPy (7.37 Wh kg^{-1}) [39], RuO_2/TiO_2 NT||AC (5.7 Wh kg^{-1}) [40], MnO_2||Fe_3O_4 (8.1 Wh kg^{-1}) [41], VO_x||VN (2.1 Wh kg^{-1}) and polypyrrole/phosphomolybdic acid||poly(3,4-ethylenedioxythiophene) /Phosphotungstic acid (4 Wh kg^{-1}) [42]. The area energy density (9.46 μWh cm^{-2}) is substantially higher than (or comparable with) those of the other fiber SCs [5,6,8,43,44] (Fig. 7d), for examples, MnO_2||CNT/carbon paper (5.4 μWh cm^{-2}) [18] and $Ni(OH)_2$||ordered mesoporous carbon (10 μWh cm^{-2}) [16]. The volumetric energy density (0.53 mWh cm^{-3}) is relatively higher than (or comparable with) those of the planar type

flexible SCs, such as, $MnO_2||Fe_2O_3$ (0.55 mWh cm^{-3}) [45] and H-TiO_2@MnO_2||H-TiO_2@C (0.3 mWh cm^{-3}) [46]. The superior capacitance and/or energy density of the fiber HSC in the current work come from the combined contribution of redox pseudocapacitance and EDLC.

Fig. 8a reveals that the electrochemical performance (CV) of the fabricated fiber HSC remains almost the same under different bending conditions. The fiber HSC exhibits excellent cycle life with a capacitance retention of 92% after repeated charge-discharge for 3000 cycles under a current of 2 mA (Fig. 8b). Fig. 8c demonstrates that the fabricated fiber HSCs were easily woven into the textile. Three such fiber HSCs connected in series are enough to power a 3.5 V red LED under normal and folded conditions (Fig. 8d and 8e). Our results show that the fabricated fiber HSCs are not only flexible, but also weaveable, with negligible decay in performance under folded condition. In addition, Fig. 8f displays the brightness variation of the powered LED at different time. It can be seen that the LED can be lighted for over 1 minute, where, initially LED is very bright but the brightness decreases after 1 minute.

4. Conclusion

In summary, $NiCo_2O_4$ nanowire (NG)-arrays were grown on CFs using a hydrothermal method and were used as positive electrode for fiber HSC. Porous carbon was prepared from *lemon peel* by hydrothermal carbonization with chemical activation and was coated on CFs to work as negative electrode for fiber HSC. With PVA/KOH as the gel electrolyte, the fabricated asymmetric fiber HSC output a voltage of 1.65 V, with a remarkable specific capacitance of 17.5 F g^{-1} (5.65 mF cm^{-1}) at 1 mA and a high energy density of 6.61 Wh kg^{-1} (9.46 μWh cm^{-2}) at a power density of 425 W kg^{-1} (608.4 μW cm^{-2}), higher than many of the previously reported values. In addition, the fabricated fiber HSC exhibits good capacitance retention of 92% over 3000 cycles. Overall, the results show that the fiber HSC has a great potential for application as a wearable energy storage device.

Acknowledgements

This work is supported by the Research Grants Council of the Hong Kong Special Administrative Region, China (Project Nos. M-PolyU503/13 and PolyU5159/13E) and the Hong Kong Polytechnic University (Project No. 1-BBA3).

Appendix A. Supplementary data
Supporting Information is available.

References:

[1] X. Lu, M. Yu, G. Wang, Y. Tong, Y. Li, Energy Environ. Sci. 7 (2014) 2160-2181.

[2] X. Cai, M. Peng, X. Yu, Y. Fu, D. Zou, J. Mater. Chem. C 2 (2014) 1184-1200.

[3] N. Liu, W. Ma, J. Tao, X. Zhang, J. Su, L. Li, C. Yang, Y. Gao, D. Golberg, Y. Bando, Adv. Mater. 25 (2013) 4925–4931.

[4] Y. Cao, M. Zhu, P. Li, R. Zhang, X. Li, Q. Gong, K. Wang, M. Zhong, D. Wu, F. Lin, H. Zhu, Phys. Chem. Chem. Phys. 15 (2013) 19550–19556.

[5] V.T. Le, H. Kim, A. Ghosh, J. Kim, J. Chang, Q.A. Vu, D.T. Pham, J.H. Lee, S.W. Kim, Y.H. Lee, ACS Nano 7 (2013) 5940–5947.

[6] Y. Meng, Y. Zhao, C. Hu, H. Cheng, Y. Hu, Z. Zhang, G. Shi, L. Qu, Adv. Mater. 25 (2013) 2326–2331.

[7] Y. Fu, X. Cai, H. Wu, Z. Lv, S. Hou, M. Peng, X. Yu, D. Zou, Adv. Mater. 24 (2012) 5713–5718.

[8] L. Kou, T. Huang, B. Zheng, Y. Han, X. Zhao, K. Gopalsamy, H. Sun, C. Gao, Nat. Commun. 5 (2014) 3754.

[9] H. Wu, Z. Lou, H. Yang, G. Shen, Nanoscale 7 (2015) 1921–1926.

[10] Q. Wang, X. Wang, J. Xu, X. Ouyang, X. Hou, D. Chen, R. Wang, G. Shen, Nano Energy 8 (2014) 44–51.

[11] J. Bae, M.K. Song, Y.J. Park, J.M. Kim, M. Liu, Z.L. Wang, Angew. Chemie - Int. Ed. 50 (2011) 1683–1687.

[12] K. Gopalsamy, Z. Xu, B. Zheng, T. Huang, L. Kou, X. Zhao, C. Gao, Nanoscale 6 (2014) 8595–8600.

[13] Q. Chen, Y. Meng, C. Hu, Y. Zhao, H. Shao, N. Chen, L. Qu, J. Power Sources 247 (2014) 32–39.

[14] F. Su, M. Miao, H. Niu, Z. Wei, ACS Appl. Mater. Interfaces 6 (2014) 2553–2560.

[15] F. Wang, S. Xiao, Y. Hou, C. Hu, L. Liu, Y. Wu, RSC Adv. 3 (2013) 13059-13084.

[16] X. Dong, Z. Guo, Y. Song, M. Hou, J. Wang, Y. Wang, Y. Xia, Adv. Funct. Mater. 24 (2014) 3405–3412.

[17] X. Wang, B. Liu, R. Liu, Q. Wang, X. Hou, D. Chen, R. Wang, G. Shen, Angew. Chemie - Int. Ed. 53 (2014) 1849–1853.

[18] H. Xu, X. Hu, Y. Sun, H. Yang, X. Liu, Y. Huang, 8 (2014) 1148-1158.

[19] S.T. Senthilkumar, R. Kalai Selvan, Phys. Chem. Chem. Phys. 16 (2014) 15692–15698.

[20] J. Zhu, J. Jiang, Z. Sun, J. Luo, Z. Fan, X. Huang, H. Zhang, T. Yu, Small 10 (2014) 2937–2945.

[21] Y. Zhang, L. Li, H. Su, W. Huang, X. Dong, J. Mater. Chem. A 3 (2015) 43–59.

[22] S.T. Senthilkumar, R.K. Selvan, Y.S. Lee, J.S. Melo, J. Mater. Chem. A 1 (2013) 1086-1095.

[23] L. Zhao, N. Baccile, S. Gross, Y. Zhang, W. Wei, Y. Sun, M. Antonietti, M.-M. Titirici, Carbon N. Y. 48 (2010) 3778–3787.

[24] S.T. Senthilkumar, B. Senthilkumar, S. Balaji, C. Sanjeeviraja, R. Kalai Selvan, Mater. Res. Bull. 46 (2011) 413–419.

[25] S.T. Senthilkumar, R.K. Selvan, J.S. Melo, C. Sanjeeviraja, ACS Appl. Mater. Interfaces 5 (2013) 10541–10550.

[26] D.U. Lee, B.J. Kim, Z. Chen, J. Mater. Chem. A 1 (2013) 4754-4762.

[27] W. Liu, C. Lu, K. Liang, B.K. Tay, J. Mater. Chem. A 2 (2014) 5100–5107.

[28] R. Zou, K. Xu, T. Wang, G. He, Q. Liu, X. Liu, Z. Zhang, J. Hu, J. Mater. Chem. A 1 (2013) 8560-8566.

[29] R. Madhu, V. Veeramani, S.-M. Chen, A. Manikandan, A.-Y. Lo, Y.-L. Chueh, ACS Appl. Mater. Interfaces 7 (2015) 15812–15820.

[30] X. Liu, S. Shi, Q. Xiong, L. Li, Y. Zhang, H. Tang, C. Gu, X. Wang, J. Tu, ACS Appl. Mater. Interfaces 5 (2013) 8790–8795.

[31] W. Zhou, D. Kong, X. Jia, C. Ding, C. Cheng, G. Wen, J. Mater. Chem. A 2 (2014) 6310-6315.

[32] Y. Zhu, C. Cao, S. Tao, W. Chu, Z. Wu, Y. Li, Sci. Rep. 4 (2014) 5787.

[33] and T.W. Daoping Cai, Dandan Wang, Bin Liu, Lingling Wang, Yuan Liu, Han Li, Yanrong Wang, Qiuhong Li, 6 (2014) 5050–5055.

[34] R.R. Salunkhe, K. Jang, H. Yu, S. Yu, T. Ganesh, S.-H. Han, H. Ahn, J. Alloys Compd. 509 (2011) 6677–6682.

[35] C. Yuan, J. Li, L. Hou, L. Yang, L. Shen, X. Zhang, J. Mater. Chem. 22 (2012) 16084-16090.

[36] C. Yuan, J. Li, L. Hou, J. Lin, X. Zhang, S. Xiong, J. Mater. Chem. A 1 (2013) 11145-11151.

[37] R. Ding, L. Qi, M. Jia, H. Wang, Electrochim. Acta 107 (2013) 494–502.

[38] G. Zhang, T. Wang, X. Yu, H. Zhang, H. Duan, B. Lu, Nano Energy 2 (2013) 586–594.

[39] V. Khomenko, E. Raymundo-Piñero, E. Frackowiak, F. Béguin, Appl. Phys. A Mater. Sci. Process. 82 (2006) 567–573.

[40] Y.G. Wang, Z.D. Wang, Y.Y. Xia, Electrochim. Acta 50 (2005) 5641–5646.

[41] T. Cottineau, M. Toupin, T. Delahaye, T. Brousse, D. Bélanger, Appl. Phys. A Mater. Sci. Process. 82 (2006) 599–606.

[42] G.M. Suppes, C.G. Cameron, M.S. Freund, J. Electrochem. Soc. 157 (2010) A1030.

[43] J. Ren, W. Bai, G. Guan, Y. Zhang, H. Peng, Adv. Mater. 25 (2013) 5965–5970.

[44] P. Xu, T. Gu, Z. Cao, B. Wei, J. Yu, F. Li, J.-H. Byun, W. Lu, Q. Li, T.-W. Chou, Adv. Energy Mater. 4 (2014) 1300759.

[45] P. Yang, Y. Ding, Z. Lin, Z. Chen, Y. Li, P. Qiang, M. Ebrahimi, W. Mai, C.P. Wong, Z.L. Wang, Nano Lett. 14 (2014) 731–736.

[46] X. Lu, M. Yu, G. Wang, T. Zhai, S. Xie, Y. Ling, Y. Tong, Y. Li, Adv. Mater. 25 (2013) 267–272.

Figure captions:

Fig. 1. Schematic illustrations of the preparation of $NiCo_2O_4$ NG@CF fiber electrode, porous carbon coated CF fiber electrode and the fabricated fiber HSC.

Fig. 2. SEM images of (a-c) as-prepared $NiCo_2O_4$ NGs on CFs (Inset of (a): photo of an as-prepared $NiCo_2O_4$ NG@CF electrode) at different magnifications. (d) Schematic representation of the morphology of $NiCo_2O_4$ NGs on a CF. (e, f) Porous carbon, at low and high magnifications, respectively.

Fig. 3. (a) TEM and (b) HR-TEM images of $NiCo_2O_4$ NG. (c) TEM and (d) HR-TEM images of the porous carbon.

Fig. 4. (a) XRD patterns of the as-prepared $NiCo_2O_4$ NG@CFs and porous carbon. (b) High resolution Co 2p XPS spectra, (c) high resolution Ni 2p XPS spectra, and (d) high resolution O 1s spectra of $NiCo_2O_4$ NG@CFs. (f) High resolution C 1s XPS spectra, and (g) high resolution O 1s XPS spectra of porous carbon.

Fig. 5. CV curves of (a) $NiCo_2O_4$ NG@CF and (b) porous carbon coated fiber electrodes at different scan rates. GCD curves of (c) $NiCo_2O_4$ NG@CF and (d) porous carbon coated fiber electrodes at different current densities 0.16, 0.20, 0.25, 0.33 and 0.41 mA cm^{-1} (corresponding currents: 1, 1.25, 1.5, 2 and 2.5 mA). (e) Specific capacitances of the electrodes at different current densities 0.16, 0.20, 0.25, 0.33 and 0.41 mA cm^{-1} (corresponding currents: 1, 1.25, 1.5, 2 and 2.5 mA), and (f) Schematic representation of charge storage mechanism of $NiCo_2O_4$ NG@CF electrode.

Fig. 6. (a) Comparison of CV curves of $NiCo_2O_4$ NG@CF and porous carbon coated fiber electrodes at a scan rate of 0.5 mV s^{-1}. (b) Digital images of the fabricated fiber HSC at normal and bending states. (c) Schematic image of the fabricated fiber HSC and the SEM images of the electrodes, with the corresponding electrochemical reactions on positive and negative fiber electrodes during charge-discharge. (d) CV and (e) GCD curves of the HSC at different operating voltages.

Fig. 7. Electrochemical performances of the fiber HSC. (a) CV curves at different scan rates, (b) GCD curves at different currents, (c) capacitance at different discharging currents, and (d) energy density *vs* power density, in comparison with reported data.

Fig. 8. (a) CV of the fiber HSC at different conditions, (b) cyclic test, (c) three fiber HSCs knitted into the fabric, (d and e) fiber HSCs connected in series power a red LED at normal and folded states, respectively, and (f) brightness variation of the LED with time. Inset of (d): enlarged image of the red LED. Inset of (e): circuit of the connection.

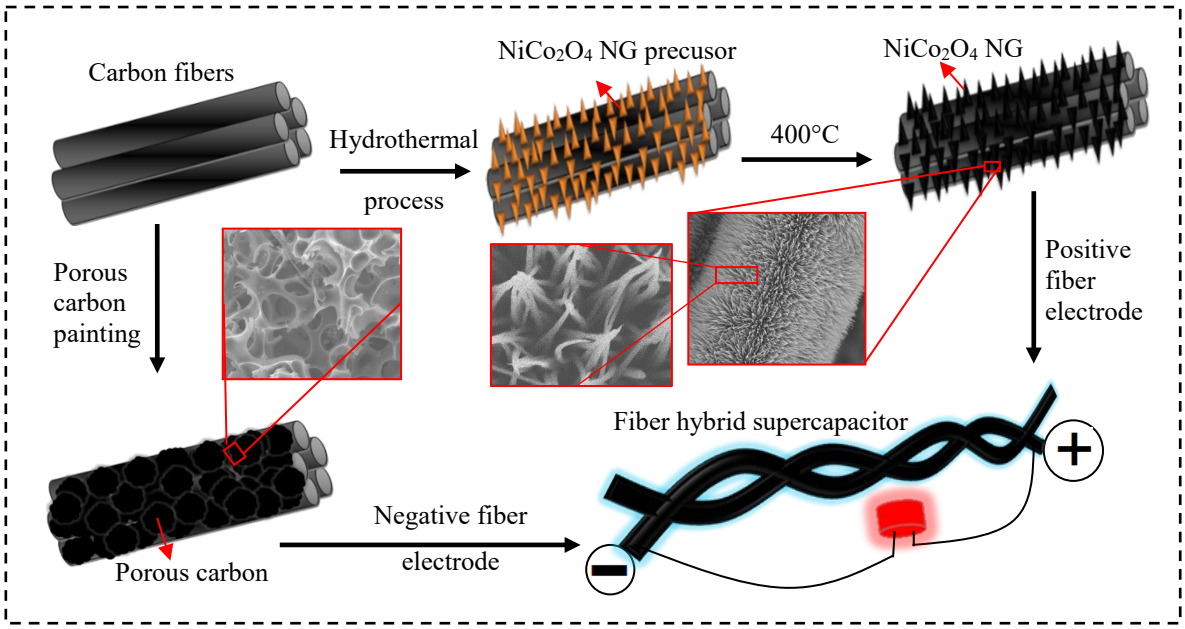

Fig. 1. Schematic illustrations of the preparation of $NiCo_2O_4$ NG@CF fiber electrode, porous carbon coated CF fiber electrode and the fabricated fiber HSC.

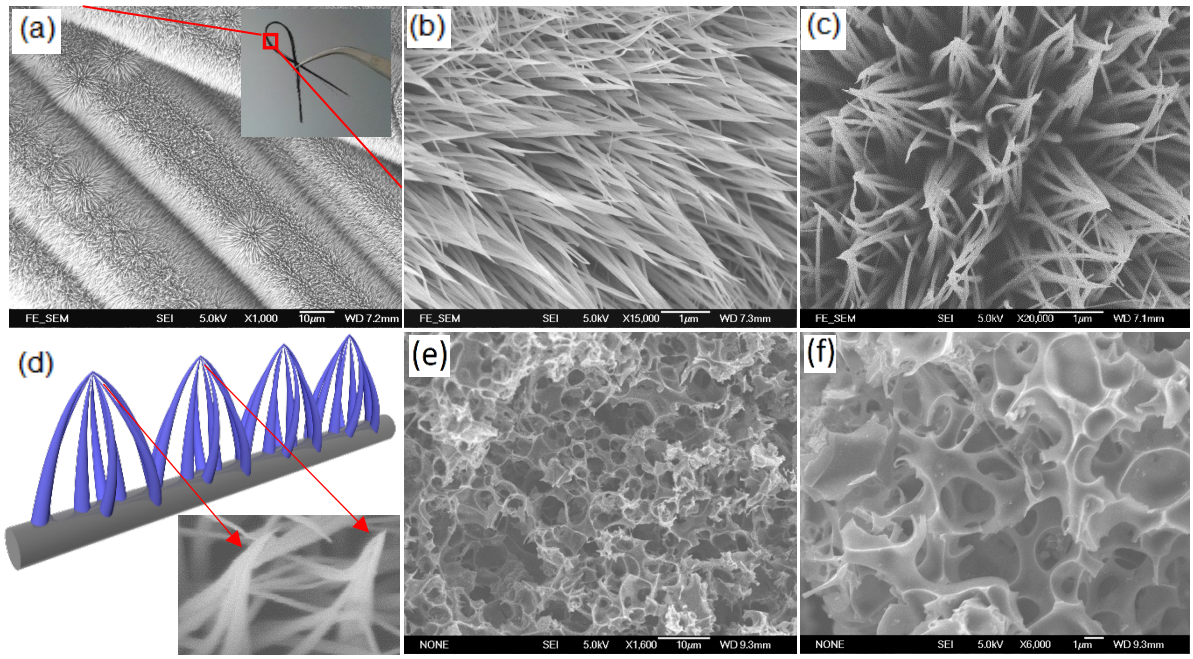

Fig. 2. SEM images of (a-c) as-prepared $NiCo_2O_4$ NGs on CFs (Inset of (a): photo of an as-prepared $NiCo_2O_4$ NG@CF electrode) at different magnifications. (d) Schematic representation of the morphology of $NiCo_2O_4$ NGs on a CF. (e, f) Porous carbon, at low and high magnifications, respectively.

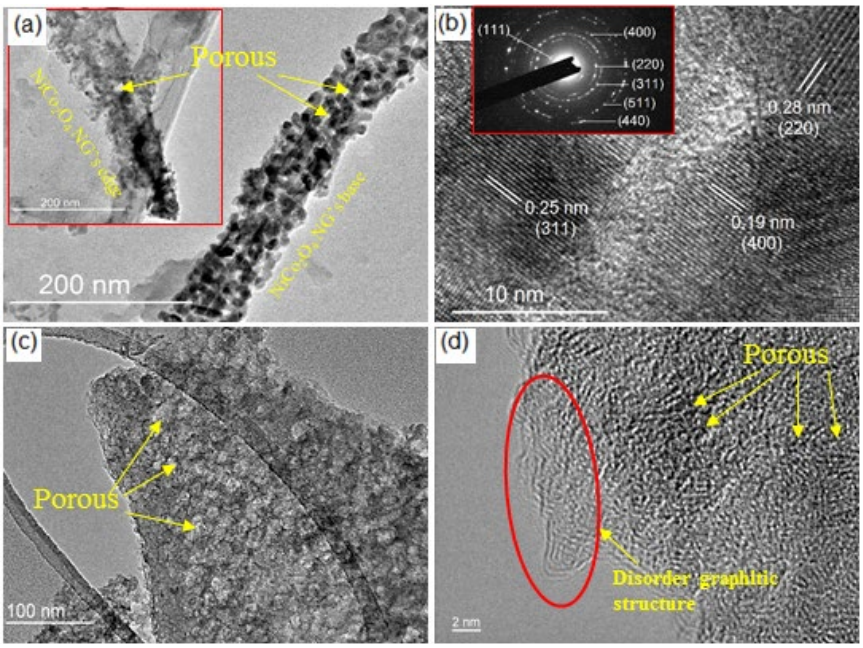

Fig. 3. (a) TEM and (b) HR-TEM images of $NiCo_2O_4$ NG. (c) TEM and (d) HR-TEM images of the porous carbon.

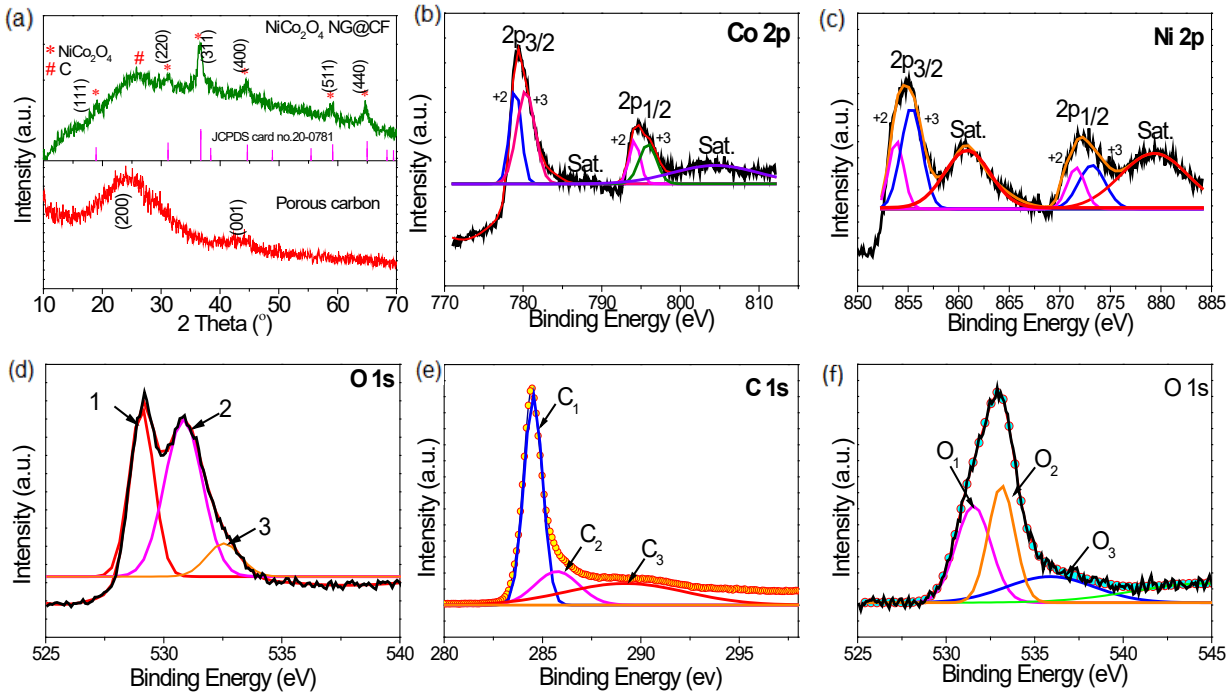

Fig. 4. (a) XRD patterns of the as-prepared $NiCo_2O_4$ NG@CFs and porous carbon. (b) High resolution Co 2p XPS spectra, (c) high resolution Ni 2p XPS spectra, and (d) high resolution O 1s spectra of $NiCo_2O_4$ NG@CFs. (f) High resolution C 1s XPS spectra, and (g) high resolution O 1s XPS spectra of porous carbon.

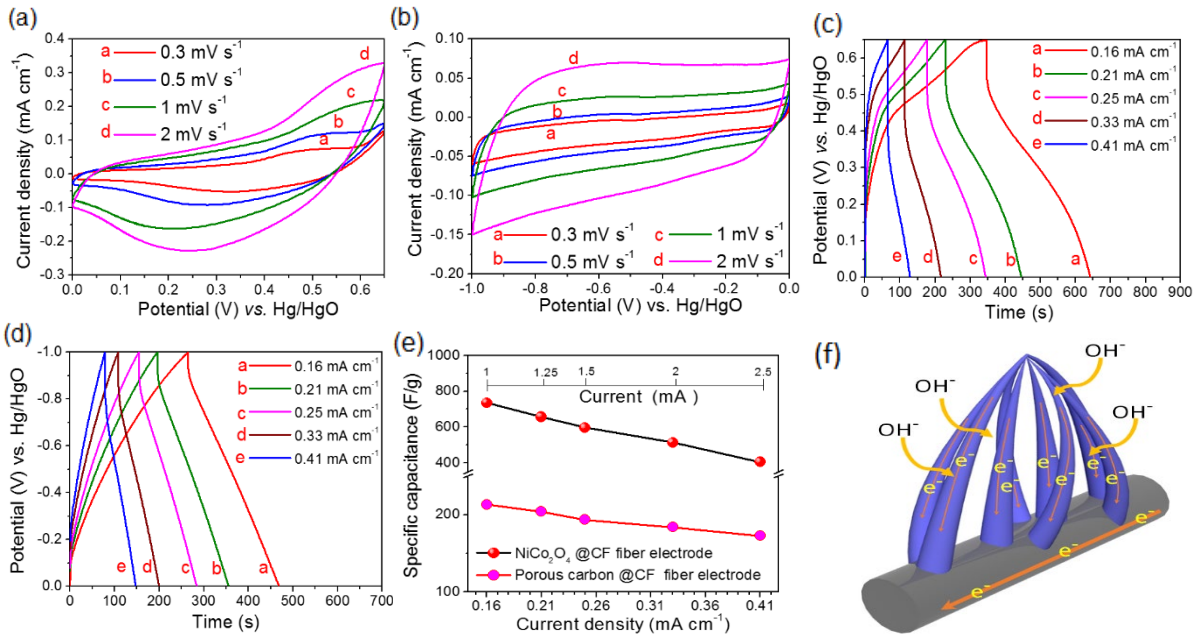

Fig. 5. CV curves of (a) $NiCo_2O_4$ NG@CF and (b) porous carbon coated fiber electrodes at different scan rates. GCD curves of (c) $NiCo_2O_4$ NG@CF and (d) porous carbon coated fiber electrodes at different current densities 0.16, 0.20, 0.25, 0.33 and 0.41 mA cm^{-1} (corresponding currents: 1, 1.25, 1.5, 2 and 2.5 mA). (e) Specific capacitances of the electrodes at different current densities 0.16, 0.20, 0.25, 0.33 and 0.41 mA cm^{-1} (corresponding currents: 1, 1.25, 1.5, 2 and 2.5 mA), and (f) Schematic representation of charge storage mechanism of $NiCo_2O_4$ NG@CF electrode.

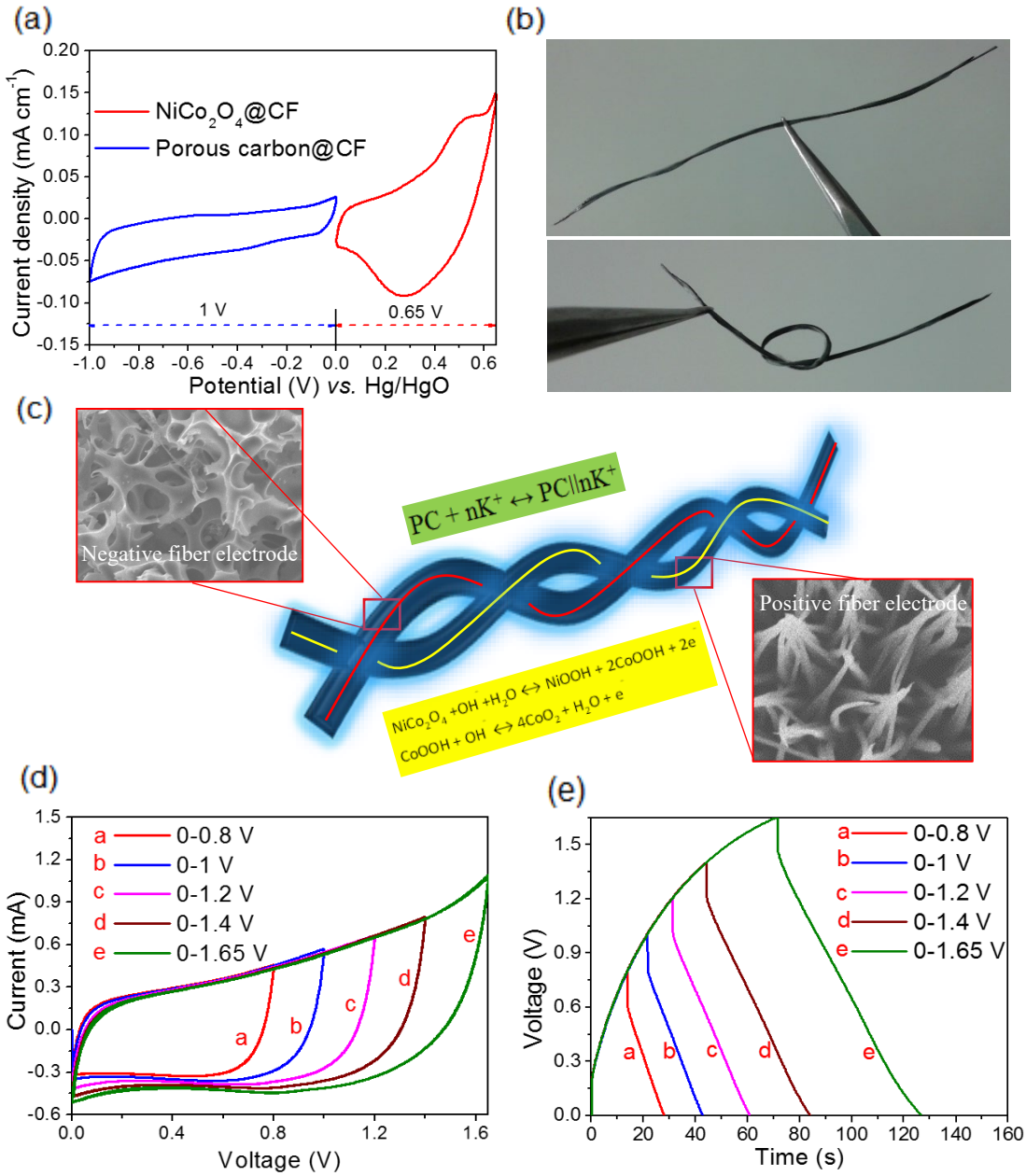

Fig. 6. (a) Comparison of CV curves of $NiCo_2O_4$ NG@CF and porous carbon coated fiber electrodes at a scan rate of 0.5 mV s^{-1}. (b) Digital images of the fabricated fiber HSC at normal and bending states. (c) Schematic image of the fabricated fiber HSC and the SEM images of the electrodes, with the corresponding electrochemical reactions on positive and negative fiber electrodes during charge-discharge. (d) CV and (e) GCD curves of the HSC at different operating voltages.

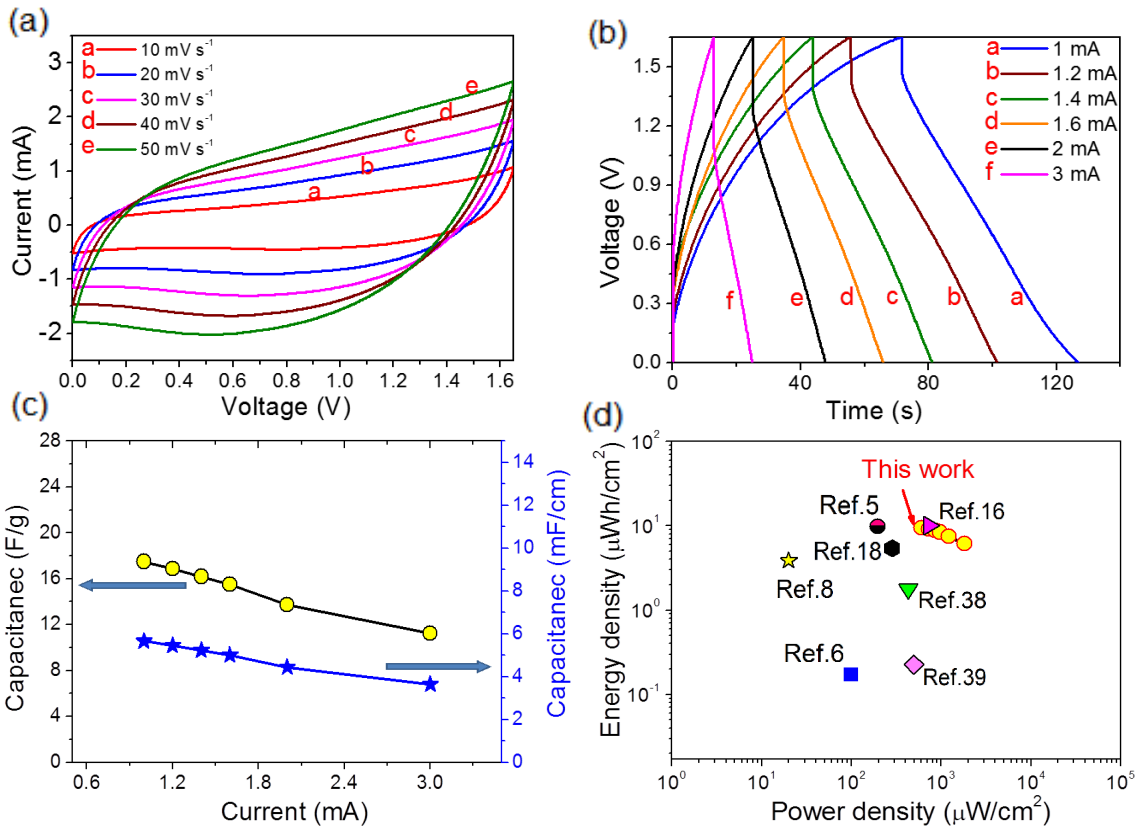

Fig. 7. Electrochemical performances of the fiber HSC. (a) CV curves at different scan rates, (b) GCD curves at different currents, (c) capacitance at different discharging currents, and (d) energy density *vs* power density, in comparison with reported data.

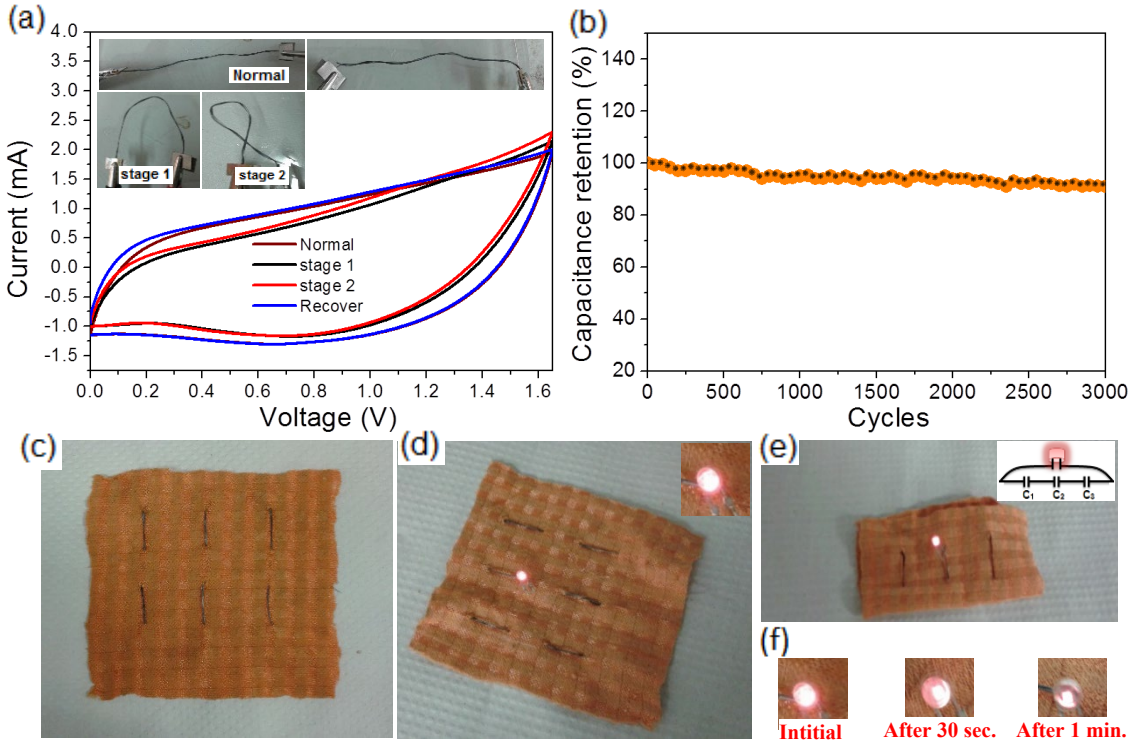

Fig. 8. (a) CV of the fiber HSC at different conditions, (b) cyclic test, (c) three fiber HSCs knitted into the fabric, (d and e) fiber HSCs connected in series power a red LED at normal and folded states, respectively, and (f) brightness variation of the LED with time. Inset of (d): enlarged image of the red LED. Inset of (e): circuit of the connection.